RSC Advances

Electrical and Lithium Ion Dynamics in Li2IrO3 from Density Functional Theory Study

Journal:	*RSC Advances*
Manuscript ID:	RA-ART-07-2014-007793.R1
Article Type:	Paper
Date Submitted by the Author:	30-Aug-2014
Complete List of Authors:	chen, yongchang; Nanchang Hangkong University, huo, miao; Nanchang Hangkong University, song, lijuan; Liaoning Shihua University, sun, zhaolin; Liaoning Shihua University,

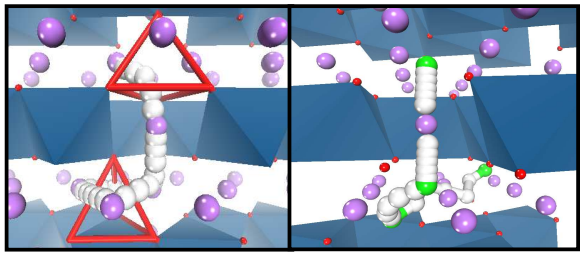

Li vacancy diffusion *Interstitial Li diffusion*

A Three-dimensional Network for the Transport of Li-related Point Defects in Layered Li_2IrO_3 Based on Fist-Principles Calculations

Electrical and Lithium Ion Dynamics in Li_2IrO_3 from Density Functional Theory Study

Yongchang Chen[1*] Miao Huo[1] Lijuan Song[2] Zhaolin Sun[2]

[1.] School of Environment and Chemical Engineering, Nanchang Hangkong University, Nanchang 330063, China

[2.] Liaoning Key Laboratory of Petrochemical Catalytic Science and Technology, Liaoning Shihua University, Fushun 113001, China

* E-mail address: chenyc828@foxmail.com

Tel: 0086-791-83863131; Fax: 0086-791-83863145

ABSTRACT

The layered Li_2IrO_3 have been investigated using the first-principles calculations within the GGA and GGA+U scheme, respectively. Within the GGA+U approach, the calculated intercalation voltage (ranges from 3.2V to 4.1V) is found to be in good agreement with experiments. Electronic-structure analysis shows that the band gap of pure phase Li_2IrO_3 is ～1eV, which is indicative of semiconductor properties. Moreover, further studies of Lithium diffusion in bulk Li_2IrO_3 shown that unlike the two dimensional diffusion pathways in rock salt structure layered cathode materials, lithium can diffuse in a three-dimensional pathway in Li_2IrO_3, with moderate lithium migration energy barrier ranges from 0.24 to 0.81 eV.

Keywords: Lithium ion batteries; Li_2IrO_3; intercalation voltage; Lithium diffusion; nudged elastic band.

1. INTRODUCTION

The performance of current cathode materials falls short of requirements for the efficient use of electrical energy in transportation, commercial and residential applications.[1] For such reason, new advances in performances are needed, which require a better understanding of known intercalation electrode materials and the discovery of new materials to ensure excellence in performance. [2-3]

The 4*d*/5*d* transition metal-containing layered oxides Li_2MO_3 (Mn, Ti, Ru, Sn, Mo, Pt) have been widely investigated as the cathode materials in lithium secondary batteries.[4-14] The oxide Li_2MO_3 have ccp oxide ion lattices with alternate basal planes of octahedral interstices occupied by only Li^+ and by $1/3Li^+$, $2/3M^{4+}$. Recently, M. Sathiya designed structurally related $Li_2Ru_{1-y}Sn_yO_3$ materials that have a single redox cation and exhibit sustainable reversible capacities as high as $230mAh\cdot g^{-1}$.[15] Moreover, they present good cycling behaviour with no signs of voltage decay and a small irreversible capacity. From a material's prospective, their research recall that the Li_2MO_3 family is rich and still largely unexplored.

Layered oxides Li_2IrO_3 is an important compound because it also can form solid solution. Many experimental investigations have been devoted to their basic properties. The deinsertion and reinsertion of Li^+ in Li_2IrO_3 is possible resulting in a reversible capacity of $\sim$135 $mAh\cdot g^{-1}$

(potential range 3−4.4 V).[16-17] X-Ray Rietveld analysis showed that Li_2IrO_3 has a layered structure with different cation layers stacking alternately along the c axis. Although numerous experimental studies have been focused on Li_2IrO_3 derivatives, little theoretical work is available in the literature concerning the lithium ion dynamics in pure phase Li_2IrO_3. First principles calculations have demonstrated their powerful capability not only of illustrating the electronic structure but also of predicting the lithium ion dynamics in electrode materials for lithium ion batteries.[18]

In this paper, we calculated the electronic structures and the average potential of layered Li_2IrO_3 within GGA and GGA+U approximation. The results demonstrate that GGA+U method gives reasonable prediction of the properties. Moreover, with the aim of understanding the lithium ion dynamic performance in pure layered Li_2IrO_3, we studied vacancy and interstitial assisted lithium diffusion in Li_2IrO_3, respectively.

2. COMPUTATIONAL DETAILS

All calculations reported herein were performed using the VASP (Vienna ab initio simulation package) code.[19-20] The projector augmented wave (PAW) method was used to model the core electrons. Li 2s, Ir 5d and 6s, and O 2s and 2p electrons are treated as valence electrons, while all the other electrons are treated as core electrons.[21] A cutoff of 520 eV was used for the plane-wave expansion of the wave function. The

Monkhorst-Pack scheme with 5×3×3 k-points meshes are used for integration in the irreducible Brillouin zone.[22]

Spin polarizations are included and the antiferromagnetic (AFM) ordering along the b-direction is used in all cases. For the exchange correlation functional, we have used the Perdew, Burke, and Ernzerhof variant of the generalized gradient approximation (GGA), together with a Hubbard-type correction to take into account the strongly correlated nature of the d electrons of the Ir atoms. Values of U = 4.5 and J =0.5 eV are used in the present study, we have tested our results against different U values, and found that the selected U and J parameters can give reasonable prediction of the average intercalation voltage. Results in Figure 3 show that the average intercalation voltage agrees quite well with experimental data. [17]The experimental crystal structures were used as the starting point of our calculations. The atomic positions were fully relaxed and the final force on each atom was less than 0.005eV/Å. The calculation of the density of states (DOS) was smeared by the Gaussian smearing method with a smearing width of 0.05 eV. To understand Li transport in Li_2IrO_3, Li-related point defects (Li vacancy and excess interstitial Li) are considered. The migration pathway is optimized using the nudged elastic band (NEB) method, with which the minimum energy paths together with the saddle points are calculated. [23-25]

3. RESULTS AND DISCUSSION

3.1 Crystal structure

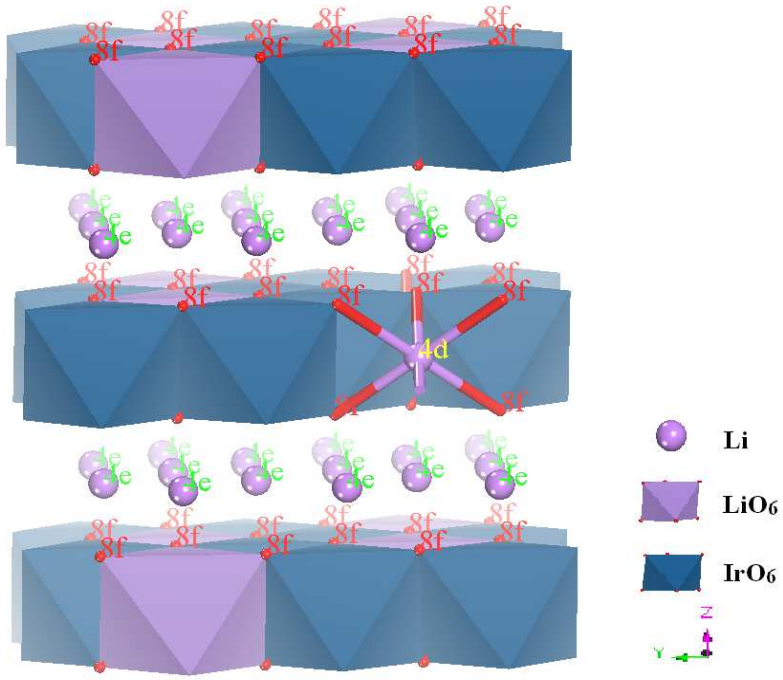

Figure 1 Monoclinic Li_2IrO_3 structure with a space group of C2/c. Two types of Li sites and one type of O sites are labeled. For the Li sites, the 4e site is in the Li layer, and the 4d site is in the $LiIr_2$ layer.

As shown in Fig.1, the structure of Li_2IrO_3 has been determined by Hironori Kobayashi et al.[17] It has an O3-type structure, which can be reformulated as $Li[Li_{1/3}Ir_{2/3}]O_2$. Tetravalent iridium and monovalent lithium comprise the Transition Metal layer, in which octahedral sites are occupied by lithium and iridium ions in proportion (1:2). Both of Lithium layer and Transition Metal layer are arranged alternately. Based on GGA and GGA+U method, we have investigated the effect of the magnetic ordering of the Iridium atoms in the structure. The antiferromagnetic (AFM) arrangement of the iridium moments is found to be lowest in energy, which is in accordance with experimental results.[17]

3.2 Electronic structure and average intercalation voltage

Using GGA+U and GGA approximation, together with an AFM ordering arrangement of Iridium atoms, we investigated the electronic structure and average intercalation voltage of Li_2IrO_3. Generally, the DFT underestimates the excited-state energies and the calculated band gaps are usually smaller than the experimental measurements. Therefore, in order to obtain more precise band-gap values from standard DFT calculations, further corrections, such as GGA+U, are needed.

Within the GGA+U approach, the electronic structure of Li_2IrO_3 is semiconductor with a gap of 1eV, and the band gap opens between the occupied O-2p states and the empty Ir-5d states.

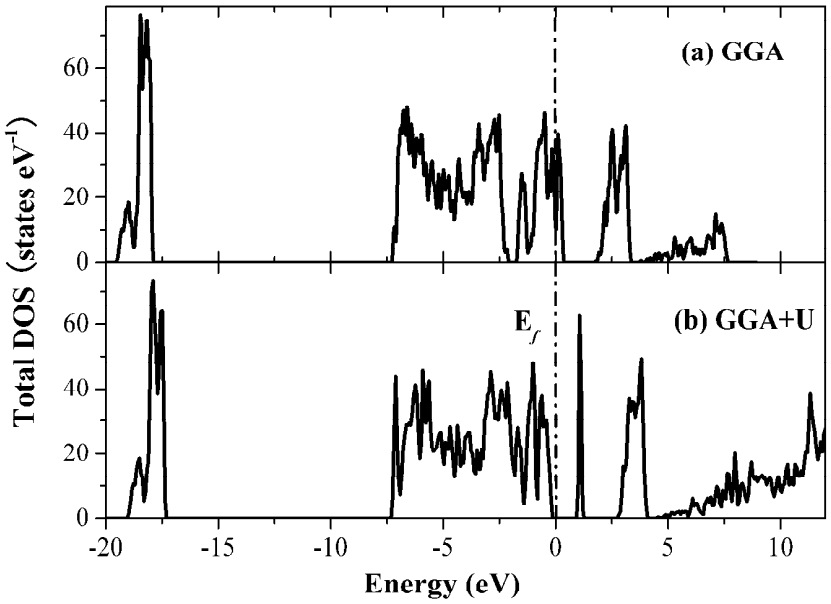

Figure 2 Total density of states of the Li_2IrO_3 .The Fermi level is set to be at zero in energy.

However, within GGA approach, the Fermi level cuts through the t_{2g} band, suggesting metallic character. Matthew has reported that the measured conductivity for Li_2IrO_3 compounds was not as high as might

be expected for a metallic conductor.[18] In fact, iridium compounds belong to the strong correlated systems, which sometimes could not be well described by GGA approximation. GGA+U method permits very accurate reproduction of electronic structure of semiconductors, including the gap which is strongly underestimated in DFT calculations.

As shown in Fig.2b, the valence band lies in the range from -7.00eV to -0.10eV below the Fermi level. Detailed orbital analysis revealed that the bands around -7.00 to -0.10 eV below the Fermi energy correspond to bonding dominantly between Ir-t_{2g} states and O-*2p* states.

To better understand the electrochemical properties of Li_2IrO_3 as cathode material for Li-ion battery, the average intercalation potential is calculated by the following Equation (1): [26]

$$V_{ave} \approx -\Delta G/nF \qquad (1)$$

where ΔG, is the difference in Gibbs free energy for the intercalation reaction, F is the Faraday constant, and n is the number of electrons (lithium ions) inserted into each unit cell. Neglecting the small changes in volume and entropy, the average intercalation potential can be approximately obtained from the internal energy, which is given by [Eq. (2)]:

$$V_{ave} \approx -\Delta E/nF \qquad (2)$$

where ΔE, is the calculated difference of the total energy. Here, the potential is investigated by the different Li^+ percentage concentration.

Considering the following chemical reaction:

$$Li_2IrO_3 \Leftrightarrow Li_{2-x}IrO_3 + xLi \quad (3)$$

then

$$\Delta E = E_{tot}(Li_2IrO_3) - E_{tot}(Li_{2-x}IrO_3) - xE_{bcc}(Li) \quad (4)$$

Where x, is the percentage concentration of extracted lithium, and $E_{bcc}(Li)$ is the metallic lithium in a body-centered-cubic (bcc) crystal structure. Within this formula, we have chosen metallic lithium as reference for the intercalation potential.

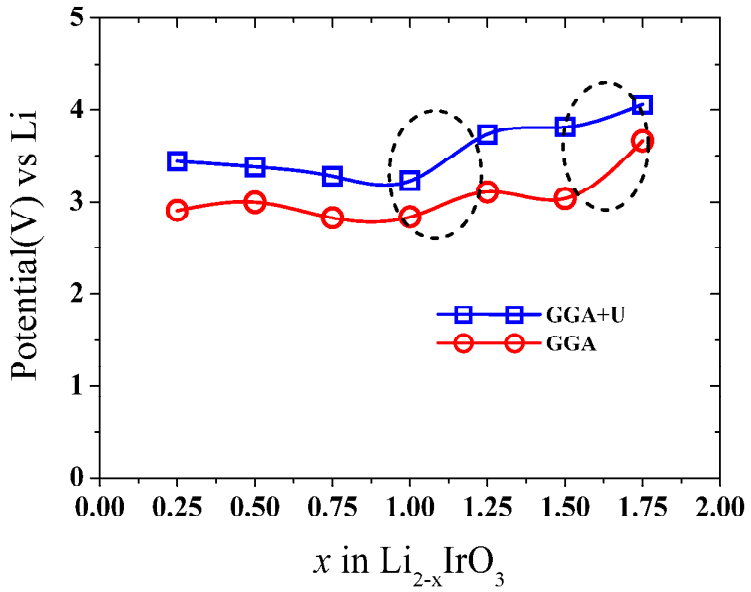

Figure 3 Comparison of the average intercalation potential of $Li_{2-x}IrO_3$calculated with the GGA+U and GGA approximation, respectively.

As seen in Fig.3, we present the calculated average intercalation potential of Li_2IrO_3 with the GGA+U and GGA approximation. Within the GGA+U approximation, the predicted average intercalation voltages are range from 3.2 to 4.1V, which is found to be in excellent agreement with experimental value.[17] However, the average intercalation potentials

calculated by GGA approximation are underestimated.

Interestingly, the extraction of lithium proceeded from x =0 to x =1.75 in $Li_{2-x}IrO_3$ with potential plateaus around 3.5 V ($0 < x < 0.75$) and 4.0 V ($1.25 < x < 1.5$), which suggests the existence of new phases at compositions with x~1.0 and 1.5. These results are consistent with XRD date on Li_2IrO_3 synthesized at 1273 K.[17]

3.3 Li Diffusion in Li_2IrO_3

The Li_2IrO_3 structure is a layered structure that possesses cation layers that alternate between pure lithium and hexagonal mixed metal ($LiIr_2$) layers. As seen in Fig.1, there are two discernible lithium sites for the Li ions in the C2/c model, i.e., at Wyckoff positions of 4e and 4d. The 4d site situated in the $LiIr_2$ layers, while the 4e sites are in the Li layers. To determine Li-ion diffusion barriers and paths, the nudged elastic band method (NEB), with GGA +U approximation, was used to calculate transition state structures.

3.3.1 Diffusion Pathways of Li vacancy

Lithium ion diffusion in layered Li_2IrO_3 occurs by a vacancy mechanism, whereby individual lithium ions hop into neighboring vacant sites. We create one Li vacancy by removing one Li from the ideal supercell of Li_2IrO_3. Lithium diffusion in the system can be represented by position exchange of the lithium ion and the vacancy. Fig.4f schematically shows all possible diffusion pathways for single lithium

diffusion in the Li_2IrO_3 lattice with the help of the lithium vacancy. There are five different migration pathways for lithium diffuses to nearby vacancy site, which are numbered 1-5 in Fig.4. These migration pathways build up a three-dimensional migration network for lithium diffusion. Fig.4(a-e) shows the corresponding energy profile along pathways (1)-(5). The energy barriers of those pathways are not quite different from each other.

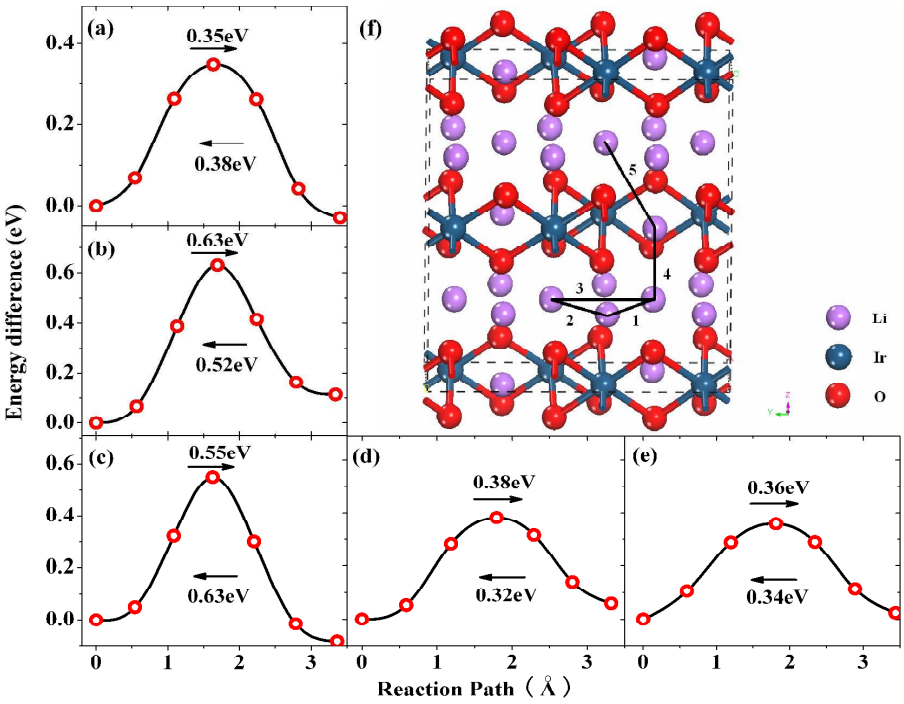

Figure 4 Energy profiles and diffusion pathways of single lithium diffusion in Li_2IrO_3 with the help of the lithium vacancy. Parts (a)-(e) are the corresponding migration energy profiles of the lithium ion diffusion along migration pathways from Nos. 1-5 that are schematically shown in part (f). The blackgreen, red, and purple spheres are Ir, O, and Li atoms, respectively. The migration pathways are marked with black line.

The energy barriers for Li^+ at the 4d site in the $LiIr_2$ plane diffusing into the 4e vacancy in the Li layer are 0.32 and 0.36 eV, respectively. (see path 4 and path 5).The hopping of the Li ion from the 4d site to the Li

plane is along a curved path passing through the oxygen tetrahedron, as shown in Fig.5.The straight path through the oxygen dumbbell site is not adopted because the distance between the oxygen dumbbell site and the nearest Iridium ion is much shorter than that between the tetrahedral site and the corresponding Iridium site. As a result, the electrostatic repulsion between Li^{+} and Ir^{4+} existing in the straight path will be larger than that in the curved one, causing a higher energy barrier than the latter.

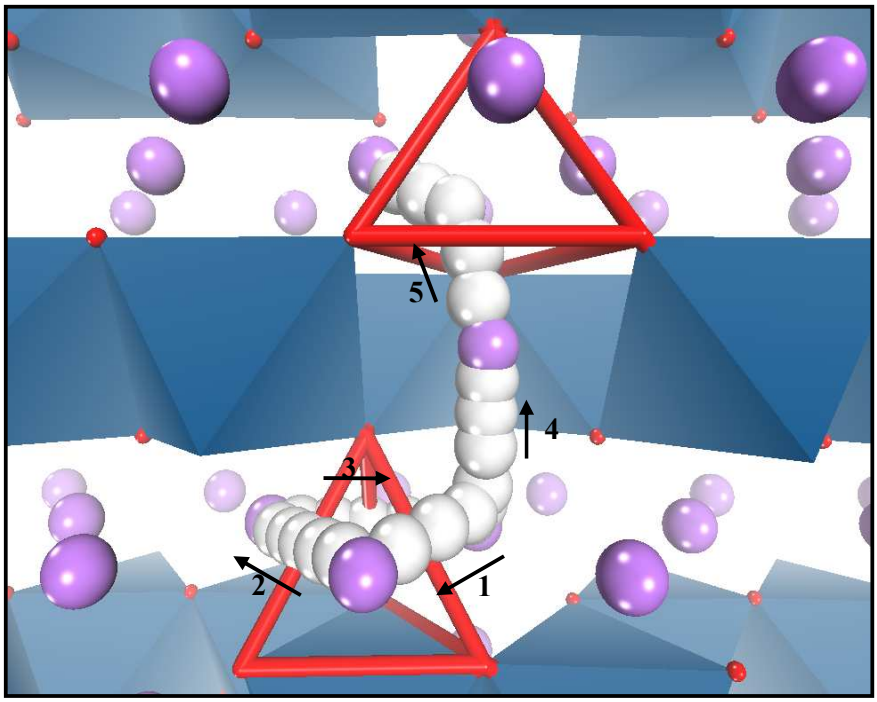

Figure 5 Diffusion pathways (small white spheres) of the five hops discussed in Figure 4, the small red spheres are O atoms, large purple spheres for normal Li, white for images during migration.

Three paths for Li^{+} diffusion in Li layer are considered. The energy barrier obtained from path 1 is low than that of path 2 and path 3. Insight about the difference between these hopping types can be obtained by investigating the specific migration pathway, as shown in Fig. 5. The Li^{+} diffuse along a straight line passing through the center of the oxygen

dumbbell in path 2 and path 3, whereas, in path 1, the Li^+ hops through the oxygen tetrahedron along a curved path. The DFT result on the energy barrier of one single vacancy diffusion in Li_2MnO_3 host is about 0.74 eV, and the pathway is a straight one through the oxygen dumbbell site. [27] This value is similar with our calculated values for Li_2IrO_3. Here, the energy barriers for Li^+ migrate from pure Li^+ layers to neighboring $LiIr_2$ are small than that of in pure Li^+ layer, which indicating Li^+ in $LiIr_2$ plane could be easier extracted than Li^+ layers. It is necessary to mention that lithium can be diffused without significant changes to the lattice, only small atomic relaxations of the nearby atoms are observed at the transition state.

3.3.2 Diffusion Pathways of interstitial lithium

There are many possible interstitial Li^+ sites in the Monoclinic Li_2IrO_3 crystal structure. It is therefore necessary to first locate the most probable Li^+ site before we consider the corresponding diffusion mechanism. The total energies calculation show that the locations of excess interstitial Li^+ between the Lithium layer and Transition Metal layer in the Li_2IrO_3 lattice. There are three different pathways for a interstitial Li^+ to switch positions with its neighboring interstitial Li^+. These pathways are labeled as (1) − (3)，as shown in Fig. 6. The energy barriers for the excess interstitial Li ion diffuse via direct hopping through spaces between the lattice sites (path1 and path2) are 0.81 and

0.72 eV, respectively.

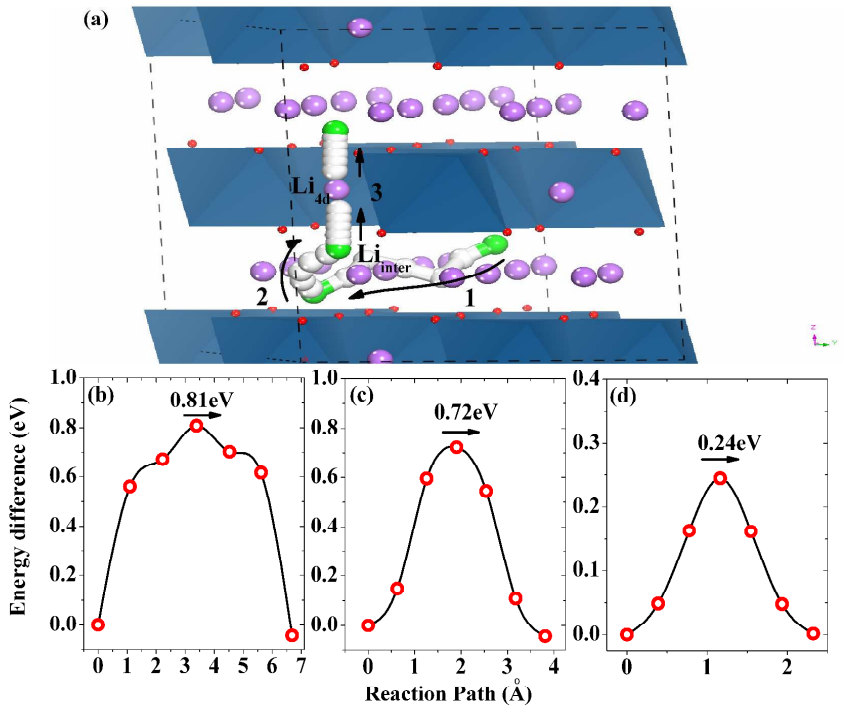

Figure 6 Energy profiles and migration pathways of interstitial lithium (Li_{inter}) migration in Li_2IrO_3. Parts (b)-(d) are the corresponding migration energy profiles of the lithium ion diffusion along migration pathways from Nos. 1-3 that are schematically shown in part (a). The large spheres (green for interstitial Li, purple for normal Li, white for images during migration), small spheres Li and O atoms, respectively. The migration pathways are marked with black line.

In the case of path 3, the pathway from one interstitial Li^+ sites to another interstitial Li^+ sites is blocked by the occupied 4d Li atom, and therefore interstitial Li^+ moving directly is not allowed. However, we find that cooperative migration is possible in this case. The interstitial Li^+ site Li hops to its neighboring 4d site, and simultaneously, the Li ion initially locates at the 4d site hops to its neighboring interstitial Li^+ sites. Fig. 6(a) and 6(c) gives the migration pathway and the migration energy barrier of this cooperative diffusion. The energy barrier is obtained to be about 0.24 eV, which indicates that interstitial Li^+ can easily diffuse across the

Transition Metal layer.

Our investigation of diffusion Pathway allows significant Li^+ motion, making the Li_2IrO_3 host a three-dimensional ionic diffuser. Moreover, from NEB calculations, the energy barrier for lithium migration along the *XY*-plane in graphite ranges from 0.308 to 0.400 eV in Li_xC_6 for different *x* values.[28] Lithium diffusion in Li_2IrO_3 seems not to be a problem in affecting the rate performance of the battery.

4. CONCLUSIONS

We have calculated the electronic structure and average intercalation voltage of layered Li_2IrO_3 with the GGA+U methodology. Predicted average voltage ranges from 3.2V to 4.1V, which are quite close to the experimental values. A simulation based on NEB method is adopted to investigate the Lithium ion diffusion in pure layered Li_2IrO_3. We found that the layered Li_2IrO_3 provides a three-dimensional network for the transport of lithium ion. The calculated lithium migration energy barrier ranges from 0.24 to 0.81 eV, which indicates the capability of Li^+ diffusion in Li_2IrO_3 is also satisfied as electrode material. Because Li_2MO_3 is a large family of compounds, theoretical and experimental efforts are still needed for optimizing the Li_2MO_3 type-structure to find new high-capacity electrodes.

Acknowledgement: The authors acknowledge the financial support from

Natural Science Foundation of China under Grant No. 21363016 and Natural Science Foundation of Jiangxi Province under Grant No. 20142BAB216030.

References

[1]. ‘‘Basic research needs for electric energy storage’’ United State Department of Energy, 2007.

[2]. Armand M.; Tarascon J. M. *Nature* 2008, **451**, 652-657.

[3]. Tarascon J. M.; Armand M. *Nature* 2001, **414**, 359-367.

[4]. Strobel P.; Lambert-Andron B. *J. Solid State Chem.,* 1988, **75**, 90.

[5]. Jansen M.; Hoppe R. *Z. Anorg. Allg. Chem.,* 1973, **397**, 279.

[6]. Riou A; Lecerf A; Gerault Y; Cudennec Y. *Mater. Res. Bull.,* 1992, **27**, 269.

[7]. Dorrian J. F.; Newnham R. E. *Mater. Res. Bull.,* 1969, **4**, 179.

[8]. Lang Von. G. *Z. Anorg. Allg. Chem.,* 1966, **348**, 246.

[9]. Hodeau J. L.; Marezio M.; Santoro A.; Roth R. S. *J. Solid State Chem.,* 1982, **45**,170.

[10]. James A. C. W. P.; Goodenough J. B. *J. Solid State Chem.,* 1988, **74**, 287-294.

[11]. James A. C. W. P.; Goodenough J. B. *J. Solid State Chem.,* 1988, **76**, 87-96.

[12]. Gopalakrishnan J.; Bhat V. *Mater. Res. Bull.,* 1987, **22**, 769.

[13]. Kumada N.; Muramatsu S.; Kinomura N.; Muto F. *J. Ceram. Soc. Jpn.,* 1988, **96**, 1181.

[14]. Asakura K; Okada S; Arai H; Tobishima S; Sakurai Y. *J. Power .Sources*, 1999, **388**, 81-82.

[15]. Sathiya M, Rousse G; Ramesha K; Laisa C. P; Vezin H; Sougrati M. T. Doublet M L; Foix D; Gonbeau D; Walker W; Prakash A. S; Hassine M. Ben; Dupont L. *Nature materials*, 2013, **12**, 827-835.

[16]. Kobayashi H; Uebou Y; Tabuchi M; Kageyama H; Yamamoto Y; Matsuoka M; Tamakib J. *J. Electrochem. Soc* 2003, **150**, A1408-A1415,

[17]. Kobayashi H; Tabuchi M; Shikano M; Kageyamaa H; Kannob R. *J. Mater. Chem*., 2003, **13**, 957–962.

[18]. Ouyang C. Y.; Zeng X. M.; Šljivancanin Ž.; Baldereschi A. *J. Phys. Chem. C* 2010, **114**, 4756–4759.

[19]. Kresse G.; Hafner. *Phys. Rev. B.* 1993, **47**, 558.

[20]. Kresse G.; Furthmuller. *J. Computational Materials Science* 1996, **6**,15.

[21]. Blöchl P.E. *Phys. Rev. B*. 1994, **50**, 17953-17979.

[22]. Monkhorst H. J.; Pack J. D. *Phys. Rev. B*. 1976, **13**:5188.

[23]. Henkelman G.; Uberuaga B. P.; Jonsson H. *J. Chem. Phys*. 2000, **113**, 9901.

[24]. Henkelman G.; Jónsson H. *J. Chem. Phys*. 2000, **113**, 9978.

[25]. Sheppard D.; Terrell R.; Henkelman G. *J. Chem. Phys*. 2008, **128**,134106.

[26]. Aydinol M.K.; Kohn A.F.; Ceder G.; Cho K.; Joannopoulos J. *Phys. Rev. B.* 1997, **56**, 1354-1365.

[27]. Xiao R. J.; Li H.; Chen L. Q. Chem. Mater. 2012, **24**, 4242.

[28]. Persson K.; Sethuraman V. A.; Hardwick L. J.; Hinuma Y.;Meng Y. S.; Ven A.; van der; Srinivasan V.; Kostecki R.; Ceder G. *J. Phys. Chem. Lett*. 2010, **1**, 1176.